Aeromechanics of Self-Twisting Blades in High-Speed Slowed Rotor Flight

Elizabeth Ward[1] **Inderjit Chopra**[2] **Anubhav Datta**[3]

University of Maryland, College Park, MD, 20742

This paper describes the effects of a composite coupled blade spar on the performance of a slowed RPM helicopter rotor in high speed edgewise flight. This study shows that antisymmetric composite coupling in the spar of a UH-60A-like rotor can provide a significant increase in the efficiency when the RPM is reduced. A comprehensive analysis was performed using a full 3D FEA based aeroelastic computational structural dynamics (CSD) solver, X3D, with the inclusion of a freewake aerodynamics model. This was first validated using existing UH-60A full-scale wind tunnel test data for high advance ratios. The current study shows that a composite blade can achieve a maximum increase in the lift to drag ratio of approximately 1.3 (20% improvement) at 85% of the nominal RPM (NR) of 27 rad/s. This efficiency gain is achieved through a combination of delayed stall drag along the retreating side of the rotor and reduced negative lift along the advancing side. A further RPM reduction to 65NR showed a maximum efficiency improvement of 15% and was attributed only to the alleviation of negative lift on the advancing side. A hygrothermally stable Winckler layup was shown to perform just as well as a nominal coupled layup at 85NR, and marginally better at 65NR, in addition to contributing to practical manufacturability of the rotor design. Close study of the strains in the rotor showed that a rotor with an extension-torsion coupled composite spar would be within the realm of practical manufacturability as the axial strains around the azimuth fell well within IM7/8552's allowable tensile strain of 6000 $\mu\varepsilon$. Tensile strain is directly related to the amount of twist change in the rotor and is reduced when the RPM is slowed and the rotor untwists towards its original cold shape.

NOMENCLATURE

a	Speed of sound, [m/s]
c	Chord length, [m]
$c_d M^2$	Sectional drag $\div \frac{1}{2}\rho a^2 c$
C_H	Rotor drag coefficient (shaft axis)
C_L	Rotor lift coefficient (wind axis)
$c_l M^2$	Sectional lift $\div \frac{1}{2}\rho a^2 c$
$c_m M^2$	Sectional moment $\div \frac{1}{2}\rho a^2 c^2$
C_P	Power coefficient
C_T	Rotor thrust coefficient (shaft axis)
C_X	Rotor propulsive force coefficient (wind axis)
E_1, E_2	Orthotropic ply Young's Moduli, [GPa]
E_{11}	Axial strain, [$\mu\varepsilon$]
G_{12}	Orthotropic ply Shear Modulus, [GPa]
K	Composite stiffness matrix
L/D_e	Lift to drag ratio, rotor efficiency
M_{ADV}	Advancing tip Mach number

[1] Ph.D. Candidate, Alfred Gessow Rotorcraft Center, Department of Aerospace Engineering
[2] Alfred Gessow Professor and Director, Alfred Gessow Rotorcraft Center, Department of Aerospace Engineering
[3] Associate Professor, Alfred Gessow Rotorcraft Center, Department of Aerospace Engineering

R	Rotor radius, [m]
t_{ply}	Composite ply thickness, [mm]
t_{spar}	Rotor spar wall thickness, [mm]
V_∞	Forward flight speed, [m/s]
α	Shaft tilt angle, [deg], positive tilt back
β_{1c}, β_{1s}	First harmonic flapping motion, [deg]
θ	Global ply orientation, [deg]
μ	Advance ratio
ρ	Air density, [kg/m^3]
σ	Rotor solidity
ν_{12}	Orthotropic ply Poisson's Ratio
ψ	Rotor azimuthal location, [deg]

INTRODUCTION

The objective of this paper is to investigate varying twist in a helicopter rotor blade caused by changing RPM in conjunction with extension-torsion composite coupling. The possibility of varying RPM in flight is a new development for edgewise rotors on emerging compound designs. It is recognized that compound helicopter designs can potentially fill the speed gap between helicopters and tiltrotors in the 180-230 kts range [1]. An efficient compound design must have at least four characteristics: a rotor efficient in both hover and high speed forward flight, a low-drag hub and fuselage, optimal load sharing (lift augmentation using wings and/or thrust sharing using propeller), and minimal aerodynamic interference losses between rotor, wing, and propeller.

A rotor optimally designed for hover (high twist) experiences high negative lift at high speeds due to flow asymmetry and high tip transonic drag and its resulting nose-down pitching moments on the advancing blade. This leads to high power requirements (low efficiency) and large vibrations. To achieve very high speeds, the rotor must slow its RPM, ideally with minimal performance and loads penalties. Slowing RPM at high speed reduces one problem (drag) but aggravates another; the very high advance ratio, μ, leads to increased flow asymmetry and even more negative lift. The twist required for an efficient rotor in high μ is very different from that required in hover [2]. Reducing the twist of the rotor in forward flight would improve the rotor efficiency.

The key question we would like to address is whether a composite extension-torsion coupled rotor is capable of changing twist in response to a change in RPM to perform well in both hover and forward flight. It will be important to examine whether current materials can withstand the stresses/strains experienced by such a rotor in the anticipated operational range, should such a rotor be built in the future.

Three kinds of composite spars with extension-torsion coupled layups were examined. First, the layups were validated with static experimental beam data. Second, a baseline titanium spar UH-60A rotor was validated with high-speed wind tunnel data. Third, the titanium spar was replaced with the coupled layups, and the effect of composite tailoring on rotor performance was studied. Finally, the strains experienced by the rotor were examined to determine the feasibility of such a design.

BACKGROUND

This research is motivated by the desire to achieve significant speed improvements in current helicopters. The element of speed is vital to the success of military missions, search and rescue, and Medevac applications. Helicopters have the unique ability to perform and operate in constrained environments so the faster and more efficient the vehicle, the larger the impact on saving lives. The Department of Defense's Future Vertical Lift initiative envisions a 50-100% increase in speed from current generation helicopters while maintaining the same hover performance.

Historically, helicopter rotor designs compromise efficiency in hover and forward flight in order to balance peak capability in both flight regimes. To be efficient in hover the rotor requires high built-in twist ($-10°$ to $-18°$), but in forward flight high twist contributes to high drag and negative lift on the advancing tip region, thereby reducing the efficiency of the rotor and speed capability of the vehicle. At high μ an ideal, efficient, rotor would have moderate to low twist.

Conventional helicopters are limited to approximately 155-160 kts by drag divergence and compressibility effects on the advancing side. These problems could be alleviated, however, if the rotor was able to reduce its RPM. In the 1970s, compound rotorcraft designs met limited success for a variety of reasons, but an important reason was the need to compromise hover performance. Today, with the advent of slowed rotor technology, there is a renewed interest in compound helicopter designs. There have also been significant advances in materials and in manufacturing processes to make a case for re-examination of composite tailoring particularly in the context of slowed rotors.

Current production helicopters, with edgewise rotors, all have a fixed RPM. However, engine technology has matured to a point where a reduction of 15% RPM is possible from engine speed alone with less than a 5% loss in specific fuel consumption. This has been a key enabler for modern high-speed demonstrators such as the Sikorsky X-2 and the Eurocopter X^3. Limited research has been done on self-twisting edgewise rotors and the prior research focused on structures alone, without aeroelastic modeling [3].

Until now, most of the research on extension-torsion coupling under RPM variation has focused on tiltrotor blades due to the fact that tiltrotors already employ a 20% reduction

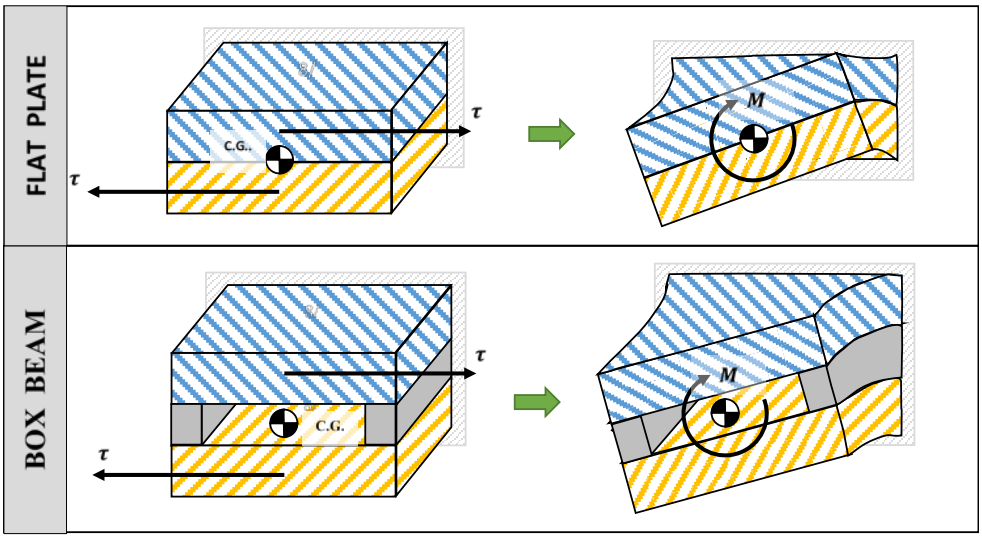

Figure 1. Mechanism of extension-torsion coupling in thin plates and its equivalent representation in a box beam type structure

in RPM between hover and cruise modes (412 RPM and 333 RPM respectively). Prior studies have shown that it is difficult to tailor tiltrotor blades to achieve a significant change in twist [4-8] without an additional weight penalty and careful inertial tuning. This is because these blades have low aspect ratios and are torsionally very stiff (~8/rev).

Edgewise rotors operate under vastly different flow conditions than tiltrotor blades due to flow asymmetry, and as such require less twist at high speed instead of more. Edgewise rotor blades are far more flexible, which means the changes in blade frequencies have a much greater impact on the rotor dynamics. They are also longer, and thus provide better centrifugal loading authority. Therefore, their behavior under slowed RPM is expected to be very different from tiltrotors.

The objective of this paper is to carry out a comprehensive analysis of an articulated rotor, similar to UH-60A, where its baseline spar is replaced with one of three composite coupled spars. First, the coupled layups and their extension-torsion behavior were validated with available experimental data. The baseline rotor was validated with high μ (up to $\mu = 1.0$), full-scale wind tunnel data. Finally, the effect of tailoring the spar was studied in detail.

DESCRIPTION OF ANALYSIS

The analyses are carried out using an integrated 3-D computational aeromechanics tool previously validated for a UH-60A-like articulated rotor [4, 5] and a V-22-like gimballed rotor, the Tilt Rotor Aeroacoustic Model [6, 7]. The solver is unique in that it uses 3-D finite element structural modeling instead of lower order beams, so the material tailoring flows down into performance, dynamic response, loads, and stresses/strains without isolated piecewise iterations between cross-sectional analysis, and beam based aeromechanics.

The rotor aerodynamic model includes C-81 airfoil tables and a lifting line model with a single rolled-up tip vortex free wake. The model includes unsteady thin airfoil theory with non-circulatory airloads. For performance calculations, the rotor was set to a fixed collective and trimmed to zero cyclic flaps (β_{1c} and β_{1s}) at the flap hinge.

Composite Modeling

This research compared two composite layup types: uncoupled and extension-torsion coupled. The uncoupled layup, denoted by 'U', is a quasi-isotropic layup where an

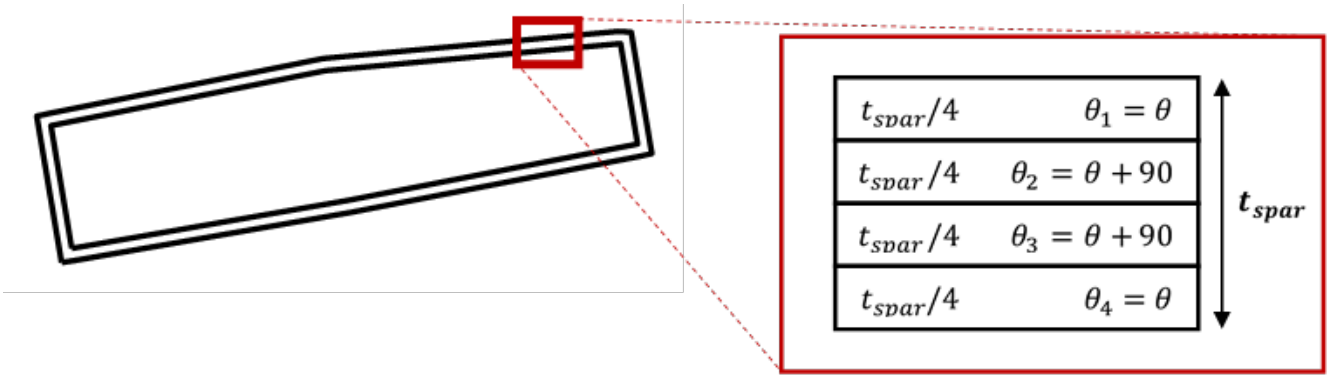

Figure 2. Application of a Winckler layup to the UH-60A box beam like spar

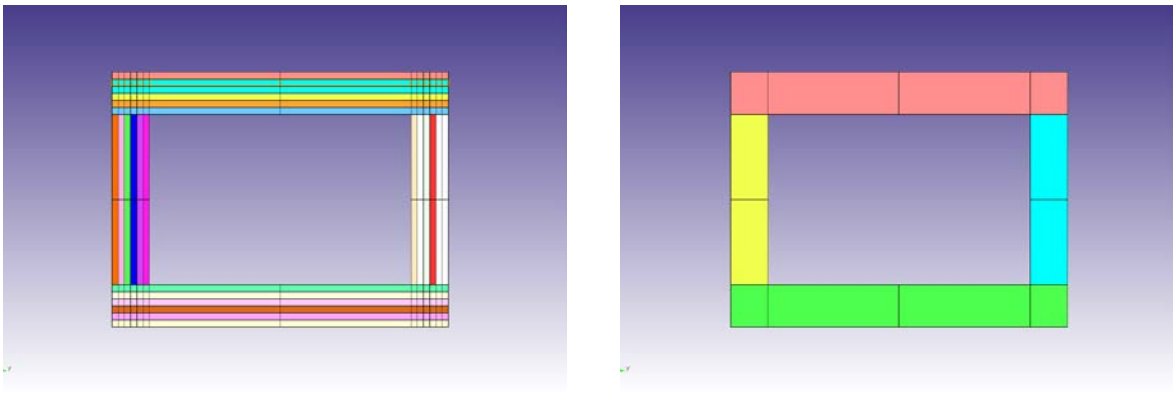

(a) (b)

Figure 3. (a) Ply resolved mesh cross section for nominal layup box beam and (b) coarse mesh cross section for nominal layup box beam. Dimensions have been magnified for clarity of elements.

axial force produces only extension. The extension-torsion layups fall under two categories: nominal antisymmetric, and hygrothermally stable antisymmetric. The result of an extension force on these composite layups is a torsional response in addition to extension. The nominal layup is one where the top and bottom plies of a load bearing structure have the same uniform ply angle, but with opposite sign. This kind of layup is denoted by 'N' (for nominal) in this paper.

A nominal layup in extreme humidity and temperature fluctuations, that might be encountered by rotor blades over the span of their lifetime, can swell, warp, and lose its material properties and structural integrity. It also has manufacturing limitations under conventional high temperature curing. Hygrothermally stable layups try to avoid these limitations. In the hygrothermally stable layups, the top and bottom of the spar still mirror each other, but consist of multiple ply orientations that are meant to provide stability from thermal or moisture fluctuations.

Two hygrothermally stable families of layups, as defined by Winckler [8] and Haynes [9], are considered here. Both Winckler and Haynes combined two layups with extension-shear coupling, that were individually hygrothermally stable, in opposite directions. The opposing shears, caused by axial loading acting at equivalent distances from the full layup's centerline, provide a purely torsional moment, as illustrated in Figure 1. In this paper the Winckler and Haynes layups are denoted by 'W' and 'H' respectively.

Winckler and Haynes applied their layups to thin, solid, plates built of 6 and 8 plies, respectively. In this research, the same principle is applied to a box beam, i.e., the layup chosen for the top and bottom of the box were both individually hygrothermally stable and provide extension-shear coupling.

The layups are summarized in Table 1. In order to maintain the same mass and minimize any inertial differences between each blade examined in this study, the rotor spar wall thickness was kept constant and then divided into elements representative of each ply orientation for a given layup. Table 1 shows that a Winckler layup requires a minimum of 4 plies on either the top or bottom to achieve hygrothermal stability, compared the Haynes layup's requirement of 3. If the spar was to be designed with the correct ply thickness there would be differences between the spar dimensions for each blade design. Instead, the spar wall thickness, t_{spar}, was held constant and the thickness of the individual ply, t_{ply}, was adjusted to fit within the original spar dimension. As an example, Figure 2 shows how the Winckler layup was applied to the rotor spar.

Table 1. Layup definition for composite spar designs used in this study

	Top Layup	Bottom Layup
U	$[0°/90°]$	$[0°/90°]$
N	$[\theta]$	$[-\theta]$
H	$[21.2°/-63.8°/-48.7°]$	$[-21.2°/63.8°/48.7°]$
W	$[\theta/(\theta+90°)_2/\theta]$	$[-\theta/(-\theta+90°)_2/-\theta]$

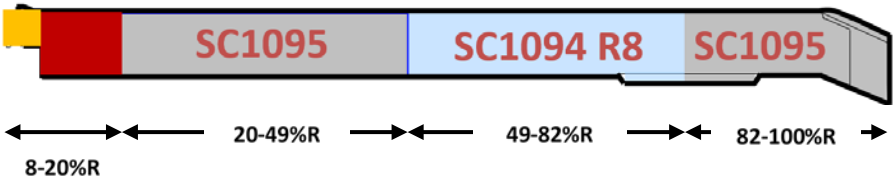

Figure 4. Distribution of airfoils along rotor span

Figure 5. Idealized UH-60A blade cross section with highlighted spar

Material Homogenization

The use of composites in 3D FEA required the consideration of how to effectively model all plies while keeping the problem size within an acceptable level. In most applications modeling each layer of a laminate results in a significant increase in the size of analysis. The material homogenization method used in this research combines the assumptions of Voigt, that all strains are uniform throughout the structure, and that of Reuss, that all stresses are uniform throughout the structure. Either of these methods, used on its own, leads to inaccurate stresses or strains at an interlaminar level.

The homogenization method used here is by Chou and Carleone [10] which assumes that the normal strains parallel to the layers are uniform (to prevent shearing) and the normal stresses perpendicular to the layers are uniform (to prevent delamination). Employing this method allows for the design of simpler models with minimal effect on performance results.

DESCRIPTION OF MODELS

Two types of models were created: beam/plate and rotor. The beam/plate models were used to validate extension-torsion coupling schemes and quantify twist sensitivity. The rotor models were used for understanding how extension-torsion coupling in the spar affects rotor performance.

Beam/Plate Models

To validate composite modeling, beam models were created for the nominal, Winckler, and Haynes layups. The nominal layup was applied to a box beam of the Chandra-Chopra box beam experiments [11]. The Winckler and Haynes layups were applied to solid plates based on their large deformation plate experiments.

For the Chandra-Chopra layups, the thin walled box beams tested were composed of 6 layers of IM7/8552 graphite-epoxy, of which the material properties are listed in Table 2. Two models were created for the box beam: one in which each individual ply was modeled (Figure 3 (a)) and one in which all plies were modeled as a single element, as shown in Figure 3 (b). A cross section of the ply resolved mesh contained 960 elements. The homogenized mesh consisted of 60 elements. Each model was designed to match the dimensions of the box beams built by Chandra et al. [11]. All elements are 27-noded, isoparametric, second order, Lagrangian hexahedral elements.

The Winckler and Haynes layups were created as per experiments conducted by Haynes [9]. The 6-ply Haynes mesh consisted of 1200 elements and the 8-ply Winckler mesh consisted of 1600 elements. The material used in these models was T300/976; its properties are listed in Table 2 and its layups listed in Table 1.

Table 2. Material properties of composite materials used in Chandra and Haynes extension-torsion coupled beam experiments

	IM7/8552	T300/976
$E_1, GPa\ (psi)$	142 (20.59e6)	125 (18.13×10^6)
$E_2, GPa\ (psi)$	9.79 (1.42e6)	8.45 (1.23×10^6)
$G_{12}, GPa\ (psi)$	6.14 (0.89e6)	4.3 (0.62×10^6)
ν_{12}	0.42	0.328
$t_{ply}, mm\ (in.)$	0.183 (0.005)	0.152 (0.006)

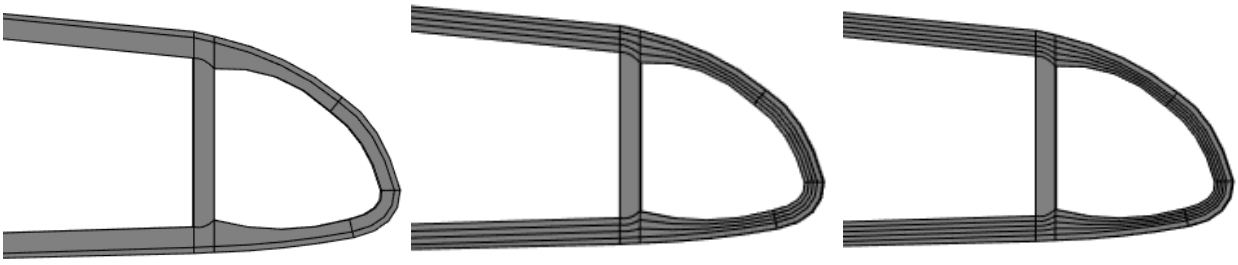

(a) Baseline/Nominal (b) Haynes, fine mesh (c) Winckler, fine mesh

Figure 6. Close up view of UH-60A-like rotor model mesh cross section for (a) homogenized model, (b) Haynes 6 ply validation, and (c) Winckler 8 ply validation

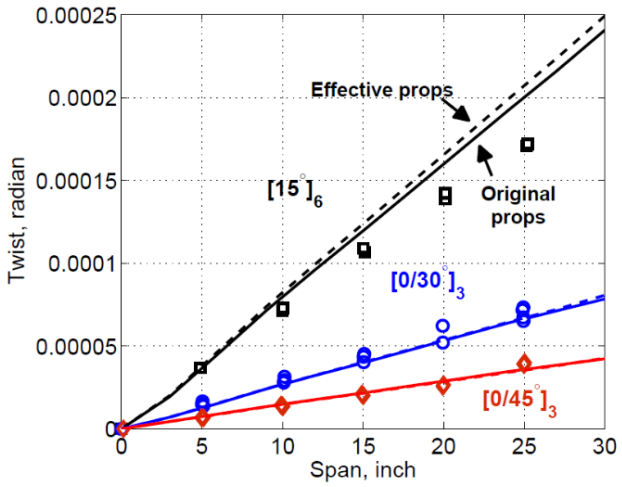

Figure 7. Twist due to a tip axial force of 1 lb for three nominal antisymmetric box beams

Rotor Models

An idealized UH-60A-like blade with a box-beam-like spar was used for the rotor model [5]. The model matches the first three modes of the UH-60A blade exactly and the higher modes approximately at the operating RPM (27 rad/s). The model has the correct geometry: hinge location, torque offset, twist, and sweep as the real rotor; only the internal construction is idealized.

The blade is made up of two airfoils: SC1095 from 20-49%R and 82-100%R, and SC1094 R8 from 49-82%R. Between 8-20%R there are no airfoils. Special consideration is needed to model this shank for high advance ratios (see VERIFICATION AND VALIDATION section).

The box beam-like section highlighted in Figure 5 is referred to as the spar and is the only part of the blade where composite material properties were applied. For the modified blades, the baseline titanium spar was replaced with IM7/8552 graphite-epoxy in either an uncoupled or a coupled layup. Although composite material weighs significantly less than titanium, the blade mass and CG were kept constant through the addition of weight in the front and rear webs. The elements defining the webs were not altered; their material density was increased to account for weight balance. This maintained uniform inertial properties between models.

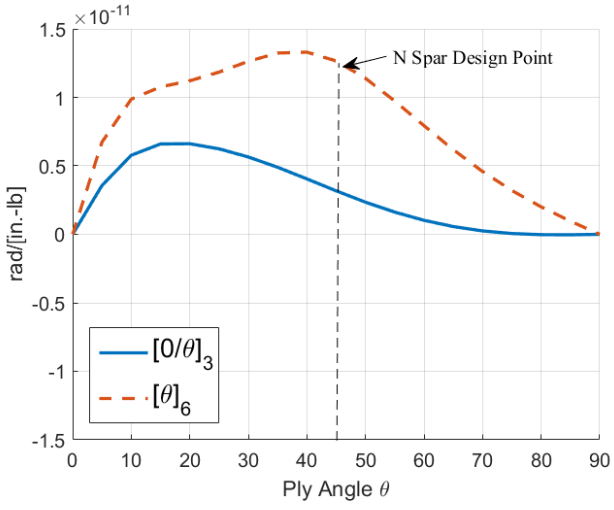

Figure 8. Twist sensitivity due to unit axial force as a function of ply angle θ for nominal box beams

As with the beam models, multiple rotor meshes were created in order to verify the homogenized model. The coarsest blade cross section, shown in Figure 6 (a), is composed of 37 hexahedral elements of 27 nodes each. The spar is composed of nine elements and is contained within, but separate from, the skin of the rotor. This model was used for all homogenized layups.

Two finer meshes were created: one for the Haynes layup (with three ply orientations), and one for the Winckler layup (with four ply orientations). These finer cross sections contained 69 and 85 elements, respectively, with the spar containing 26 and 32 of them. Also highlighted in Figure 6 (a-c) is that the mesh refinements were only made in the thickness direction of the spar.

VERIFICATION AND VALIDATION

Verification of the composite homogenization process and validation of the model accuracy were required before application of the extension-torsion coupling to the rotor. This was carried out for both the beam/plate and rotor models. Validation of high-μ aerodynamic modeling was performed on the baseline (titanium spar) rotor model using NASA/Ames high-μ, 40 ft x 8ft full-scale wind tunnel tests.

Beam Models

Validation of the beam models was performed using the experimental results produced by Chandra, et al.[11]. Three antisymmetric layups were considered. Two of the beams tested were defined by a $[0/\theta]_3$ layup. These experiments provide validation of the analysis, as well as validation of the material homogenization employed to simplify the structural model. Figure 7 shows the twist along the beam span due to an axial tip force of 1 lb for three different layups with both the ply resolved and homogenized meshes. For the exception of the $[15]_6$ case, homogenization has minimal impact on the results. In general, predictions match the experimental data for the $[0/30]_3$ and $[0/45]_3$ cases extremely well.

In order to select the nominal coupled layup for the rotor model, a simple cross sectional analysis was used to understand the effect of ply angle on the stiffness properties of the rotor spar. Equation 1 shows the simplified linear relationship between axial force and torsion moment about the x-axis and beam strain and rate of elastic twist. For $M_x = 0$, Equation 2 shows the relationship between axial force, F_x, and twist rate. While $K_{1,4}$ represents the extension-torsion coupling, the actual twist due to a given extension force – the twist sensitivity – is determined also by the torsional stiffness, $K_{4,4} = GJ$, that allows for twist, and the extensional stiffness, $K_{1,1} = EA$, that induces twist.

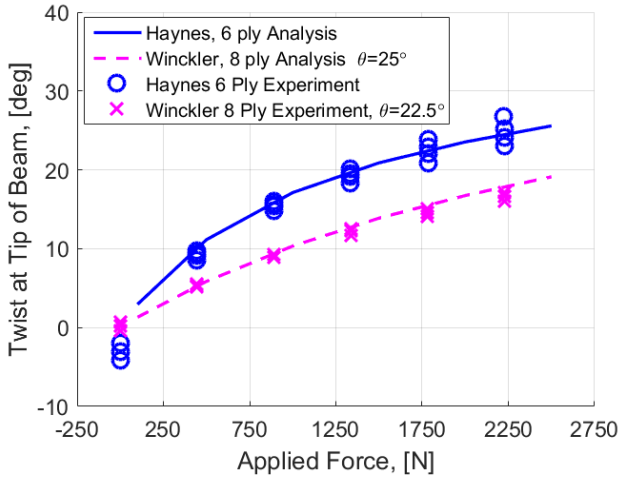

Figure 9. Experimental vs. analytical results for twist as a function of applied axial loading

$$\begin{Bmatrix} F_x \\ M_x \end{Bmatrix} = \begin{bmatrix} K_{1,1} & K_{1,4} \\ K_{1,4} & K_{4,4} \end{bmatrix} \begin{Bmatrix} u_e' \\ \phi' \end{Bmatrix} \quad (1)$$

$$\phi' = \frac{K_{1,4}}{K_{1,1}K_{4,4} - K_{1,4}^2} F_x \quad (2)$$

Figure 8 shows the twist sensitivity for the beams validated in Figure 7. It is clear why the experimental data showed the $[15]_6$ case had more twist than the $[0/30]_3$ or $[0/45]_3$ cases – the sensitivity of pure $[\theta]_6$ layups is higher than the mixed $[0°/\theta]$ layups. Maximizing twist sensitivity is important for the purpose of this work so a pure $[\theta]$ layup with $\theta = 45°$ was chosen for the rotor spar.

Validation of the hygrothermally stable beam models was required a nonlinear analysis due to large deformations. Figure 9 shows predictions compared to experimental data by Haynes. Nonlinearity of strain/displacement was important for predicting these large deflection tests; in essence K is now a function of displacement. Twist sensitivity of Winckler layups of varying θ is shown in Figure 11; $\theta = 25°$ was chosen.

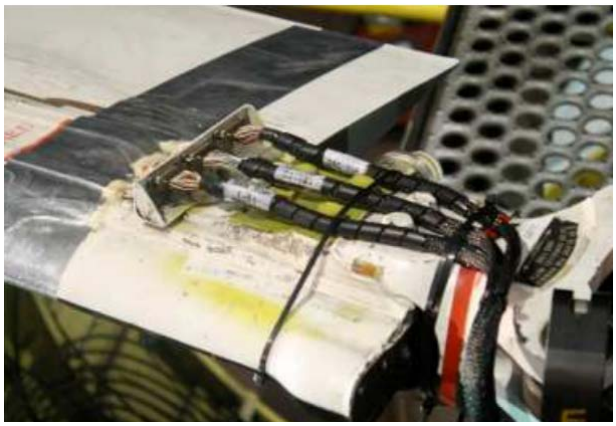

Figure 10. UH-60A instrumented blade shank

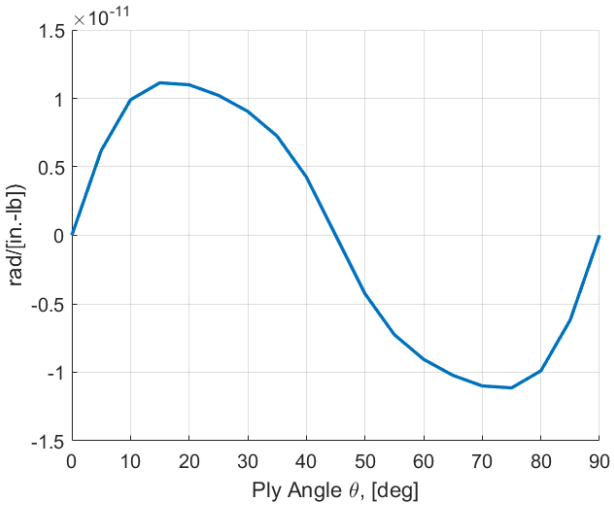

Figure 11. Twist sensitivity due to unit axial force as a function of ply angle θ for Winckler hygrothermally stable layup

Baseline Rotor Model

The baseline (titanium spar) rotor model was validated with experimental results from a full-scale, slowed RPM, high-μ, UH-60A rotor [12] tested in the Ames, 40 ft x 8ft full-scale wind tunnel in 2010. Validation at high-μ required careful consideration of the highly instrumented blade root end, shown in Figure 10.

The blade shank is an unfaired drag producing structure extending from 8-13%R, with a transition to blade airfoils from 13-20%R. The nominal blade airfoils were shown in Figure 4. The shank has been accounted for in the analysis by a correction to the drag tables of the SC1095 airfoil.

Contemporary analyses report significant deficiencies in predicted performance without the use of a shank drag correction. However, the magnitude of the corrections are ad hoc and depend strongly on the tool being used. Yeo [13] used a shank drag coefficient of 0.4 for 8-13%R and 0.02 for 13-20%R to match measured performance at high-μ. Ormiston [1] assigned a drag coefficient of 1.5 across both segments. Potsdam modeled the blade shank using a first principles approach (CFD) which suggested a drag coefficient between 0.14-0.18, however drag on the non-aerodynamic blade could not be calculated [14].

The current analysis found that a shank drag coefficient of 0.75 provided good correlation of rotor efficiency at the highest advance ratio of $\mu = 1.0$. Figure 12 shows how the predicted and measured rotor efficiency, L/D_e, compared at different thrust levels. Rotor efficiency, L/D_e, is defined by Equation 3. The L/D_e trends match very well at high advance ratios and acceptably well at low advance ratios. It should be noted, however, that the analysis consistently over-predicted the maximum L/D_e and the range of C_T/σ experienced by the rotor at all advance ratios, regardless of shank drag.

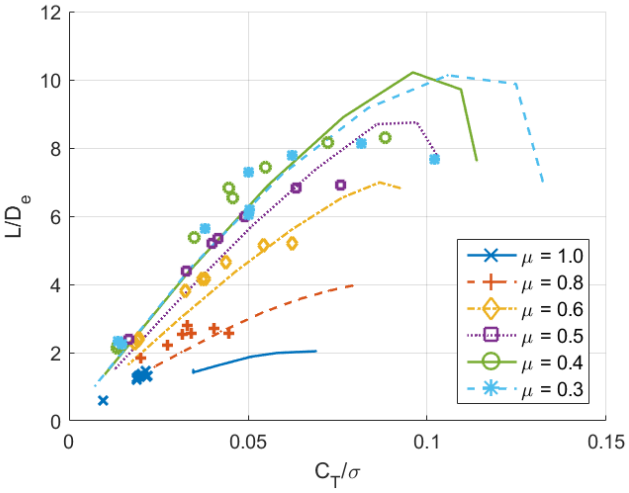

Figure 12. Analytical vs. experimental results for rotor efficiency vs. blade loading for a UH-60A rotor with a titanium spar at an RPM of 10.8 rad/s and various advance ratios

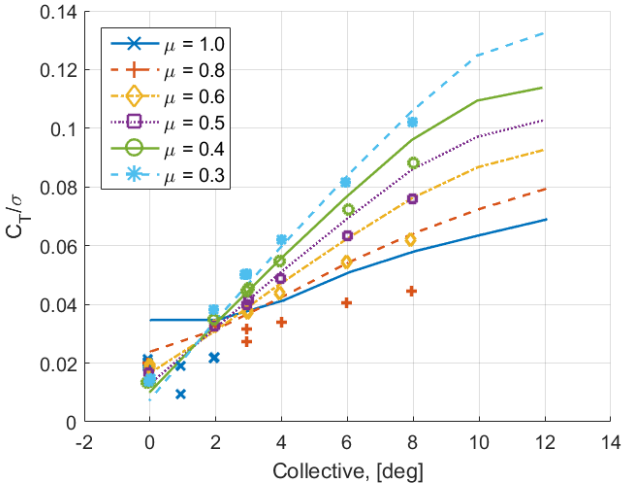

Figure 13. Analytical vs. experimental results for C_T/σ as a function of collective for a UH-60A rotor with a titanium spar at an RPM of 10.8 rad/s and various advance ratios

$$\frac{L}{D_e} = \frac{C_L}{\frac{C_P}{\mu} - C_X} = \frac{C_T}{\frac{C_P}{\mu} + C_H} \tag{3}$$

at zero shaft angle when $C_L = C_T$ and $C_X = -C_H$

Figure 13, Figure 14, and Figure 15 show how the prediction of thrust, C_T/σ, drag, C_H/σ, and power, C_P/σ – the contributing components of L/D_e – varying with collective, compared to experiments. The predictions, though not perfect, capture the correct trends and provide adequate confidence in the model and the solver to study the effect of composite coupling in the rotor.

Composite Rotor Model

As was carried out with the beam models, it was important to verify that the use of material homogenization did not influence the performance predictions. This was especially important for the hygrothermally stable designs as each ply in the layup is oriented at a different angle. Comparison of the ply resolved and homogenized meshes for all three composite spar designs (in Figure 6) shows that performance is not affected by material homogenization of the spar elements, see Figure 16.

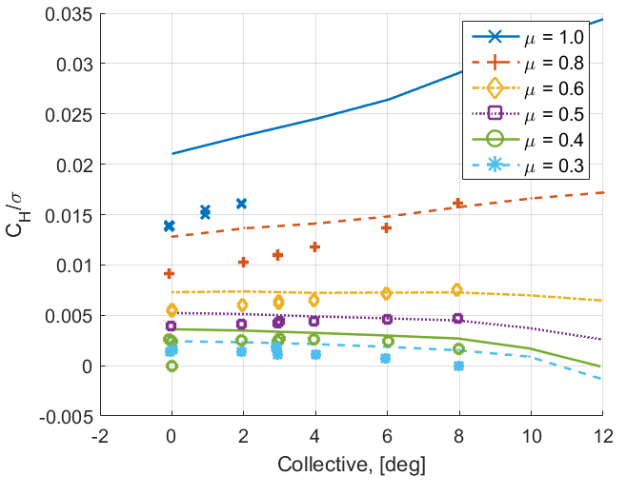

Figure 14. Analytical vs experimental results for C_H/σ as a function of collective for a UH-60A rotor with a titanium spar at an RPM of 10.8 rad/s and various advance ratios

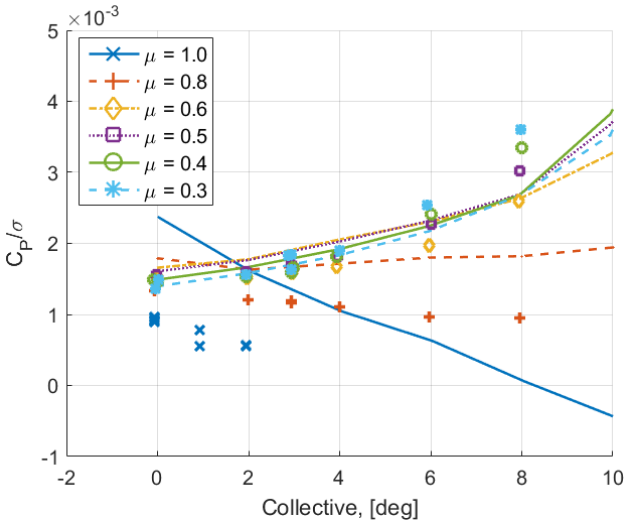

Figure 15. Analytical vs. experimental results for C_P/σ as a function of collective for a UH-60A rotor with a titanium spar at an RPM of 10.8 rad/s and various advance ratios

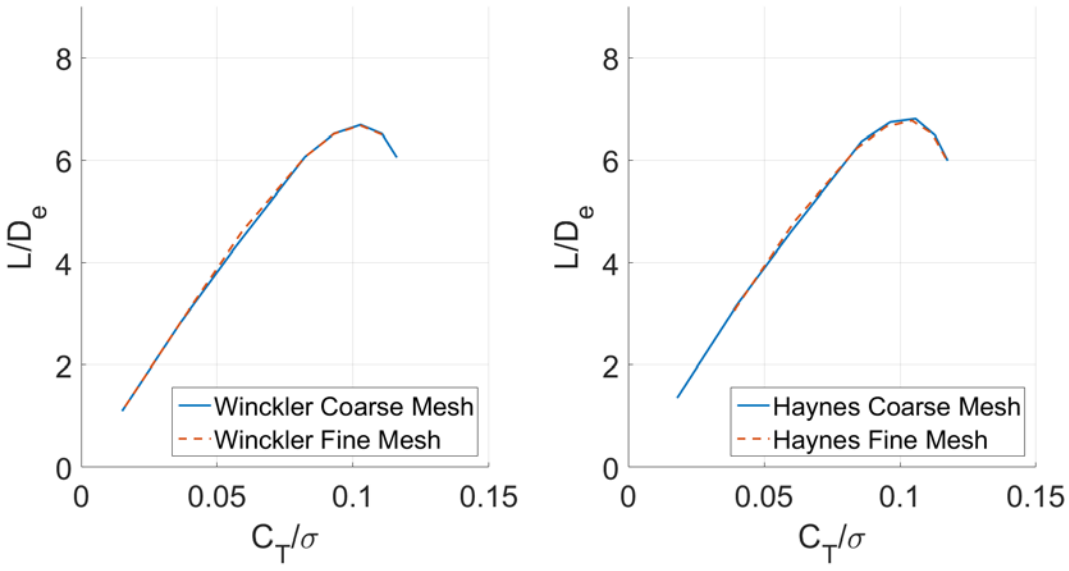

(a) Winckler mesh **(b) Haynes mesh**

Figure 16. Comparing performance of coarse, homogenized material mesh to fine, ply resolved mesh for Winckler layup ($\theta = 25°$) and Haynes layup at 100NR

RESULTS

The effect of composite coupling on rotor performance was studied by examining the following:

1) Effect of coupling on radial twist distribution
2) Comparison of uncoupled to nominal coupled rotor at 100NR
3) Comparison of uncoupled to nominal coupled rotor at reduced RPM (85NR, 65NR)
4) Effect of hygrothermally stable layups on rotor performance

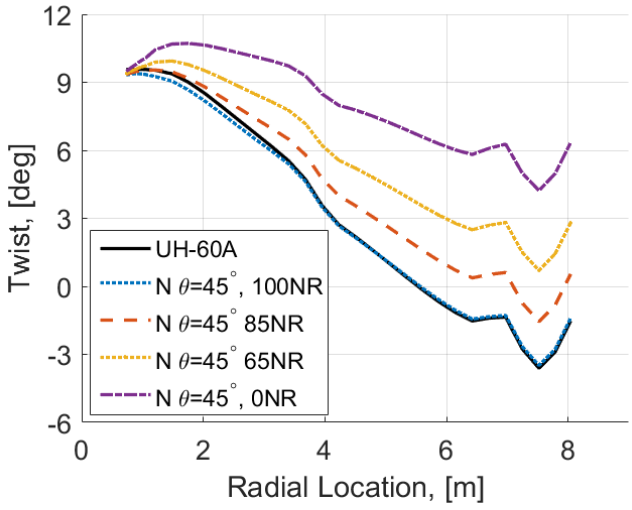

Figure 17. Twist as a function of radial location for baseline titanium spar UH-60A blade compared to twist of rotor with a nominal layup composite spar at 100NR, 85NR, and 65NR. Calculated in vacuum.

Variation in rotor twist was calculated in vacuum. Analysis of the rotor in forward flight was carried out at a speed of 157 kts and a constant rotor shaft tilt of $\alpha = 0°$.

Effect of Coupling on Radial Twist Distribution

To ensure that the coupled spar rotors matched the twist of the baseline titanium spar rotors at 100NR and that they untwisted as the rotor RPM was slowed, the following method was employed:

1. Apply the composite coupling to the baseline spar in the opposite direction of intended actuation (top is now $[-\theta]$ and bottom is $[\theta]$).
2. Spin this blade in vacuum at 100NR and record the final twist distribution.
3. Redefine the composite mesh with the recorded twist distribution, and correct the direction of composite coupling (top returns to $[\theta]$ and bottom to $[-\theta]$).
4. Verify the correct twist is achieved by spinning the new blade at 100NR and comparing the twist distribution to that of the baseline titanium spar blade.

As shown in Figure 17, as the rotor is slowed, the natural reduction in centrifugal loading allows the rotor to return to its cold shape twist.

Effect of Nominal Layup on Performance at 100NR

The measure of efficiency in forward flight is the lift to drag ratio, L/D_e. In order to make a consistent comparison, the results for the coupled composite rotor spar are compared

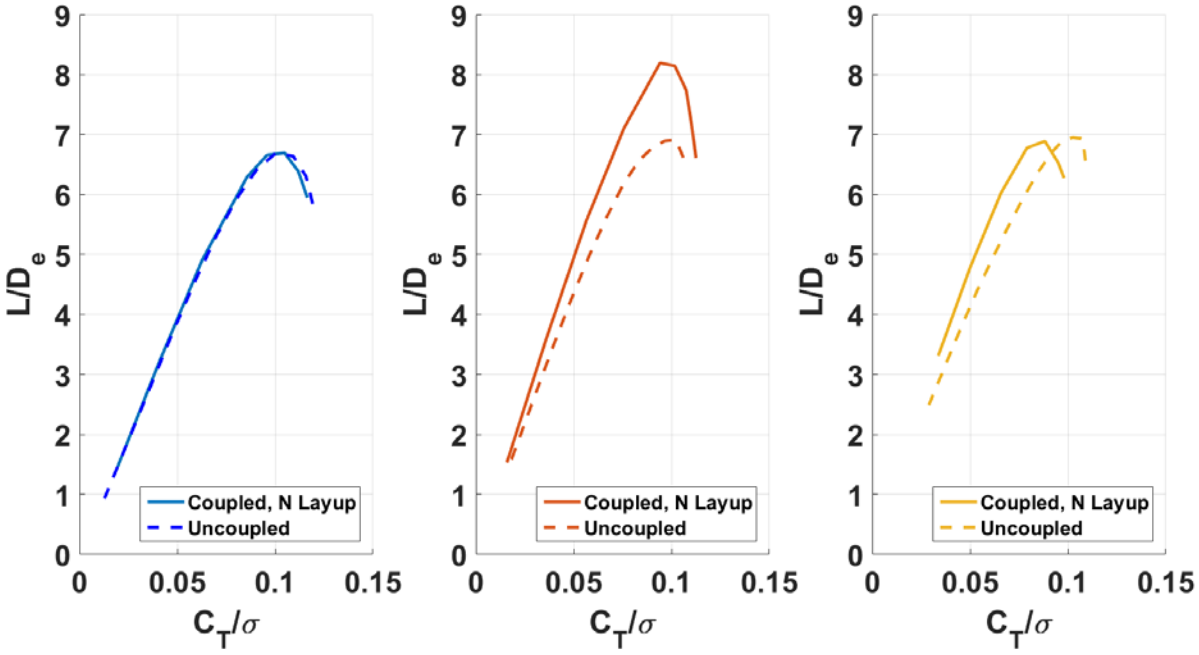

(a) 100NR, $\mu = 0.37$ (b) 85NR, $\mu = 0.46$ (c) 65NR, $\mu = 0.57$

Figure 18. L/D_e ratio for uncoupled and nominal coupled rotors for (a) 100NR, (b) 85NR, and (c) 65NR

to a blade with an uncoupled composite spar, instead of the baseline titanium spar. This ensures that any performance differences found subsequently are due to composite structural coupling alone.

At the full hover RPM, 100NR (27 rad/s), the efficiency of all blades must remain the same. This was ensured by reproducing the UH-60A twist distribution at 100NR, as well as the baseline titanium spar's rotor mass and sectional c.g. locations. As can be seen in Figure 18 (a), the L/D_e for both the uncoupled and nominal coupled rotors is the same at 100NR for all blade loadings, C_T/σ.

Effect of Nominal Layup on Slowed RPM Performance

When the rotor RPM is slowed to 85NR, see Figure 18 (b), while both rotors see an increase in efficiency it is clear that the coupled rotor outperforms the uncoupled rotor at all blade loadings, reaching a max L/D_e of 8.2 compared to the uncoupled rotor's maximum of 6.9. When the RPM is slowed further to 65NR (Figure 18 (c)), the coupled rotor again outperforms the uncoupled rotor but only at lower blade loadings. The coupled and uncoupled rotors at 65NR only reach a peak L/D_e ratio of 6.9.

To understand the cause of the performance change between the uncoupled and coupled rotors, Figure 19 considers lift versus drag at two different radial locations (75%R and 89%R) and three different RPMs. Although there are differences between the three RPM at 75%R (a and c), the effects are more clearly outboard at 89%R (b and d). Two conclusions can be drawn from this figure: 1) the drag has more distinct differences as the rotor RPM is varied and 2) there is variation in negative lift between the uncoupled and coupled rotors.

Figure 20 shows the azimuthal variation of drag. For both the uncoupled rotor and the coupled rotor, a reduction in RPM from 100NR to 85NR yields a very large reduction in drag along the advancing side of the rotor. Further RPM reduction to 65NR yields a relatively smaller reduction. For the uncoupled rotor, a significant drag spike appears in the retreating side of the rotor at 85NR. For the coupled rotor this spike is eliminated. At 65NR the uncoupled rotor shows a rapid increase in drag along the advancing side. For the coupled rotor this increase is eliminated, but a spike on the retreating side appears.

As the rotor RPM is reduced from 100NR to 85NR the advancing tip Mach number decreases from $M_{ADV} = 0.89$ to $M_{ADV} = 0.80$, so the blade tip leaves the transonic region when the rotor is slowed. This change in operating environment alone, with or without composite coupling in the blade spar, would result in a substantial reduction in drag. In addition to this change in M_{ADV}, the coupled rotor is also untwisted (as shown in Figure 17). This reduces the drag on the rotor as the aerodynamic environment does not change significantly ($M_{ADV} = 0.80$ to $M_{ADV} = 0.66$).

Figure 21 shows how Mach number and angle of attack, AoA, vary along the azimuth. At any given RPM, between uncoupled and coupled, the Mach number range does not change. This is an indication that compressibility is not a factor in the rotor efficiency change due to composite coupling. The main factor is the change in AoA distribution. This figure shows that the uncoupled rotor at 85NR and the coupled rotor at 65NR enter stall conditions ($AoA > 15°$)

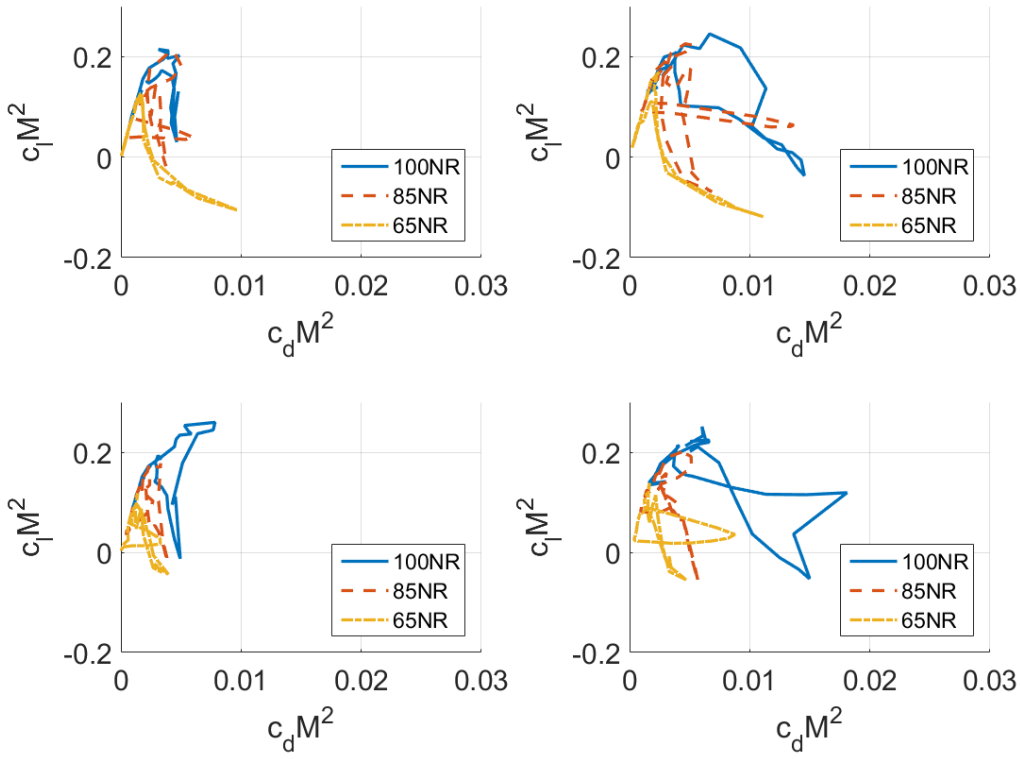

Figure 19. Lift vs drag for the uncoupled and nominal coupled rotor at two radial locations (75%R and 89%R) and three nominal RPM (100NR, 85NR, and 65NR). Calculated in vacuum.

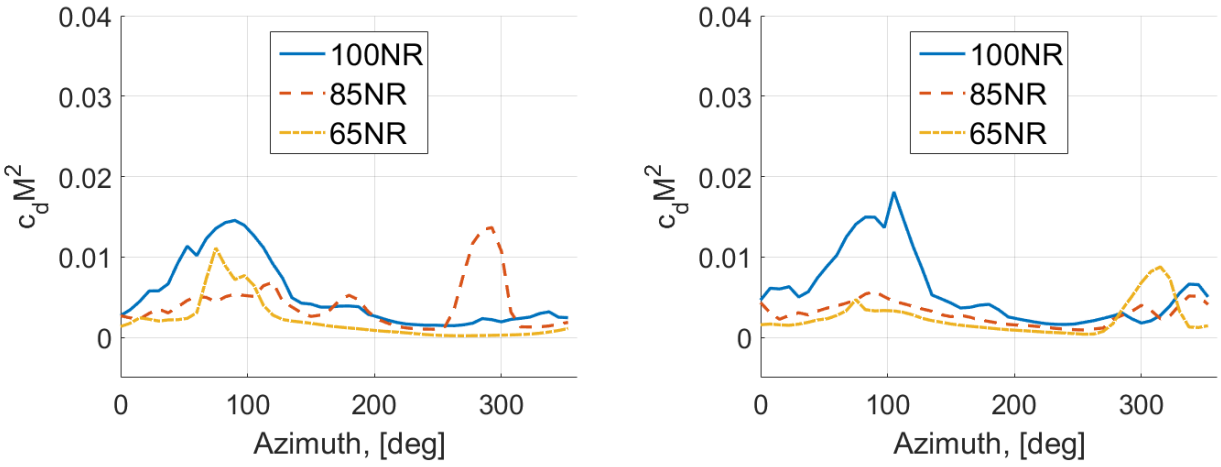

(a) Uncoupled, 89%R **(b) Coupled N ($\theta = 25°$), 89%R**

Figure 20. Drag as a function of azimuth at $C_T/\sigma \approx 0.1$ for uncoupled and nominal coupled rotors at 89%R for 100NR, 85NR, and 65NR

along the retreating side of the rotor. This accounts for the spikes in the drag coefficient at 65NR that were seen in Figure 20.

The second observation made from Figure 19 is that there are variations in the negative lift between the uncoupled and coupled rotors. These have a significant impact on the rotor performance. Figure 22 shows the azimuthal variation of lift. Again, both the uncoupled and coupled rotor have very similar distributions at 100NR, as expected. When the rotor RPM is reduced to 85NR, however, the uncoupled rotor generates significantly more negative lift on the advancing side of the rotor, whereas the coupled rotor does not. This effect is only important outboard of 90%R.

It should be noted that the choice of the nominal layup with $\theta = 45°$ for this study was made to achieve maximum untwisting of the rotor blade, but was not optimized to

maximize the aerodynamic performance at multiple slowed RPMs. It is possible that a different layup angle could have and the nominal layup with $\theta = 45°$ outperform the Haynes

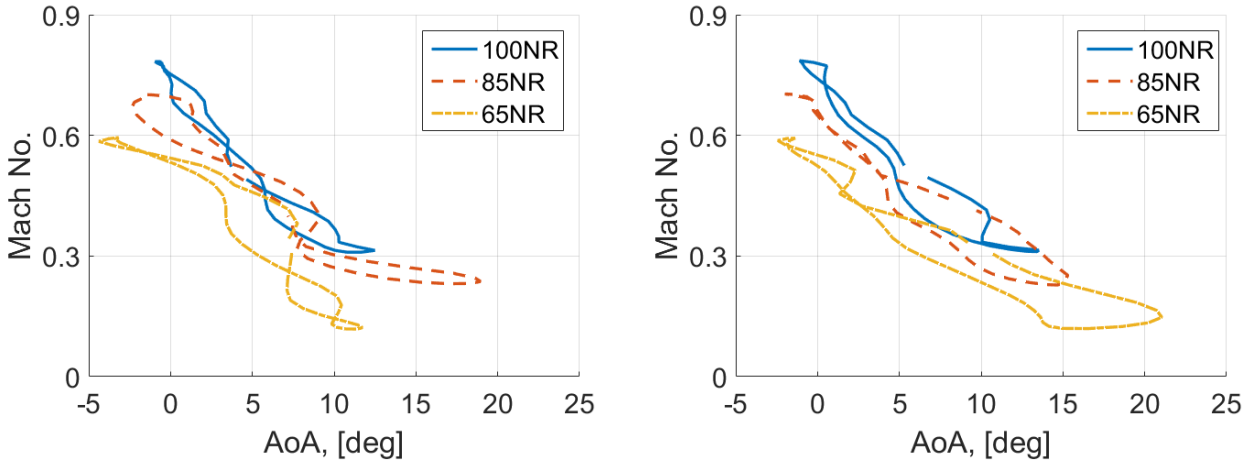

(a) Uncoupled, 89%R **(b) Coupled Nominal ($\theta = 25°$), 89%R**

Figure 21. Mach number as a function of angle of attack at $C_T/\sigma \approx 0.1$ for uncoupled and nominal coupled spar rotors at 100NR, 85NR, and 65NR

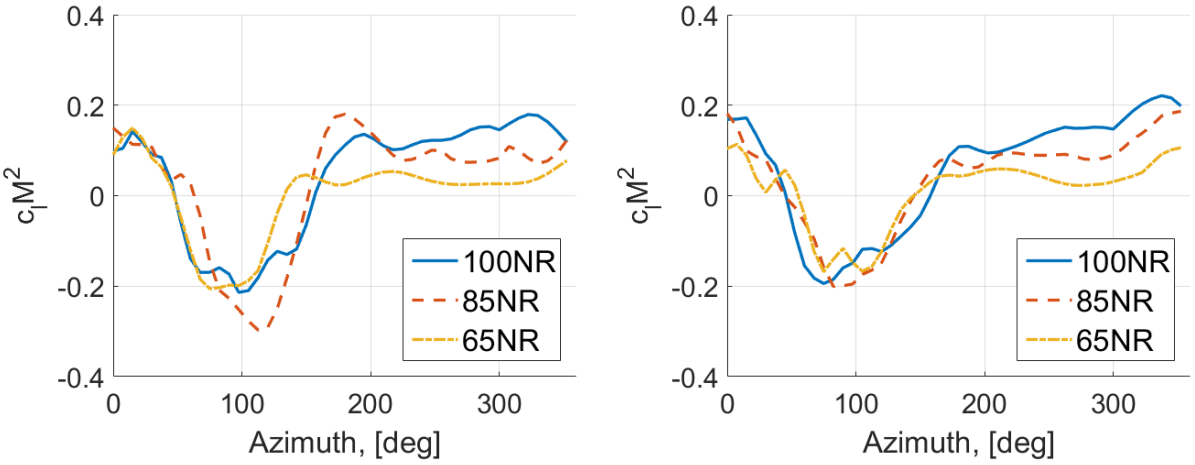

(a) Uncoupled, 89%R **(b) Coupled Nominal ($\theta = 25°$), 89%R**

Figure 22. Lift as a function of azimuth at $C_T/\sigma \approx 0.1$ for uncoupled and nominal coupled rotors at 89%R for 100NR, 85NR, and 65NR

provided an increase over the uncoupled rotor L/D_e ratio at 85NR *and* 65NR if the change in twist was less extreme.

Effect of Hygrothermally Stable Layups on Rotor Performance

The hygrothermally stable layups, when applied to the same box beam spar, once again affected the twist of the rotor strongly, as shown in Figure 23. The Winckler layup achieved twist very similar to the nominal layup; the Haynes layup twisted relatively less.

At 100NR, shown in Figure 24 (a), there are no discernable differences between the rotor performance of the three coupled and uncoupled rotors. When the rotor RPM is reduced, see Figure 24 (b), the Winckler layup with $\theta = 25°$ layup at $\mu = 0.46$, with a maximum L/D_e difference of 0.3 at $C_T/\sigma \approx 0.1$. When the RPM is slowed to 65NR the Winckler layup outperforms both the nominal and Haynes blades by 0.3 and 0.5 respectively, at their peak ($C_T/\sigma \approx 0.09$).

Figures 25 and 26 show the lift and drag variations of the Winckler blade compared to the nominal blade. The differences between the two are hardly discernible, which indicates that including hygrothermal stability does not significantly alter the rotor behavior. Of the 3 studied, it was determined that the Winckler layup provides the best performance, improving L/D_e at both slowed RPMs, relative to the uncoupled blade.

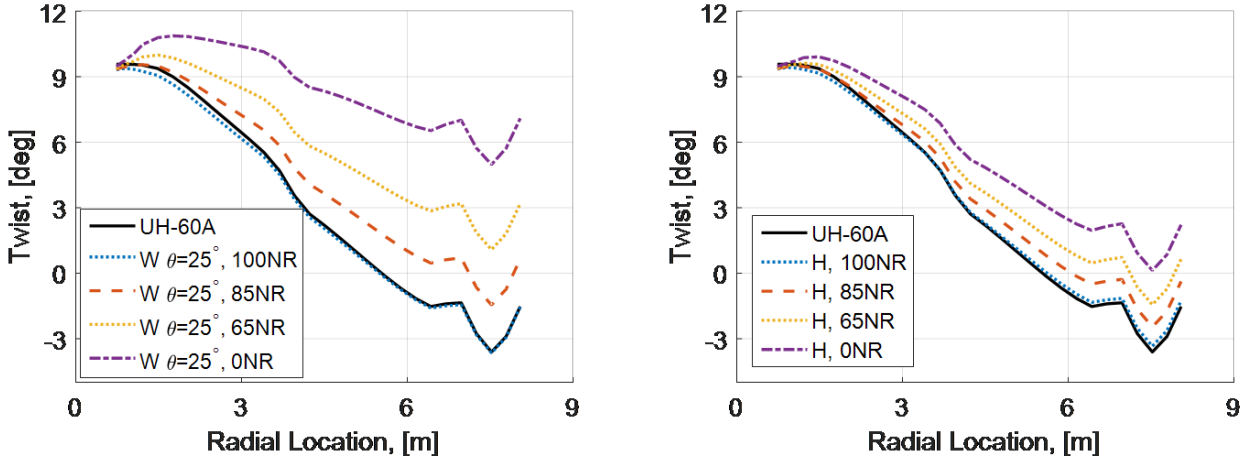

(a) Winckler Layup **(b) Haynes Layup**

Figure 23. Twist as a function of radial location in vacuum for (a) Winckler layup spar with $\theta = 25°$ and (b) Haynes layup spar

Composite Spar Strains

Practical design requires that strength constraints of the materials be met. The material considered here, IM7/8552, has allowables of approximately 6000 microstrain (με) in tension, 4500 $\mu\varepsilon$ in compression, and 3000-4500 $\mu\varepsilon$ under cyclic loading [2] in the fiber direction. Figures 27 through 29 show a qualitative view of the global radial strains that the uncoupled and Winckler blade experiences at 100NR. Transformation of strain from the blade frame to the fiber direction plane can be done using Equation 4.

$$\varepsilon_x' = \varepsilon_x \cos^2\theta + \varepsilon_y \sin^2\theta + \varepsilon_{xy}\sin(\theta)\cos(\theta) \qquad (4)$$

For the coarse, homogenized spar meshes there is no applied ply angle between the global and fiber frame, as the calculated material properties include the different ply orientations. The Winckler blade utilizes four different ply orientations to ensure hygrothermal stability. When both the fine and coarse global strain results were transformed into the coordinate's corresponding ply direction, Figure 30 (a) shows that the difference in the fiber strain between both is minimal.

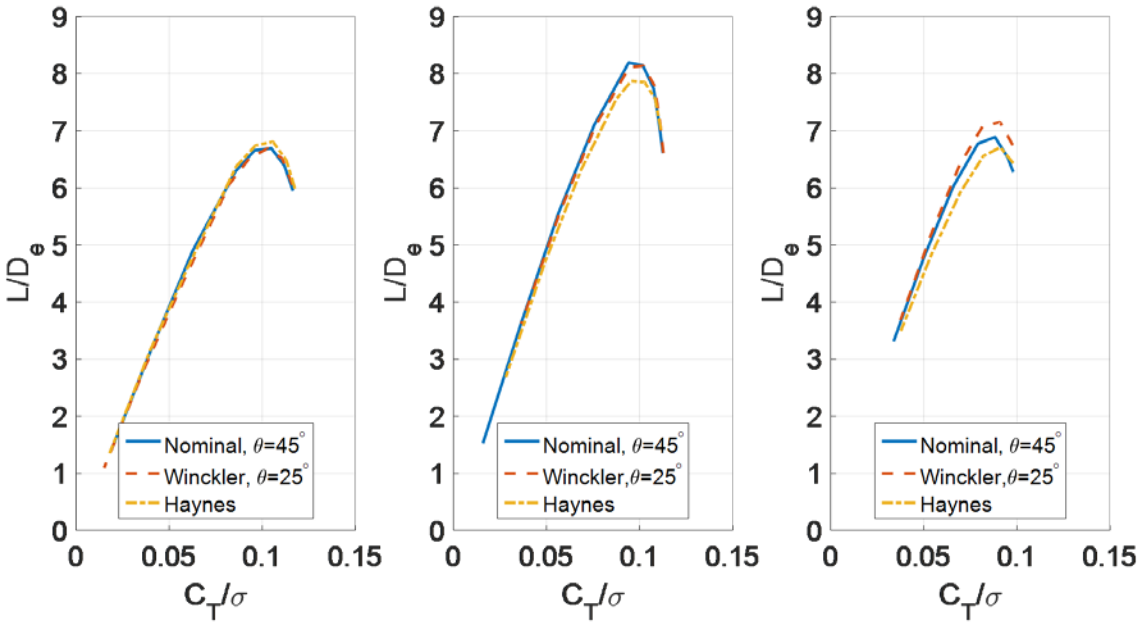

(a) 100NR, $\mu = 0.37$ **85NR, $\mu = 0.46$** **(c) 65NR, $\mu = 0.57$**

Figure 24. L/D_e ratio vs. blade loading for Chandra-Chopra composite spar design compared to the hygrothermally stable designs of Winckler and Haynes at (a) 100NR, (b) 85NR, and (c) 65NR

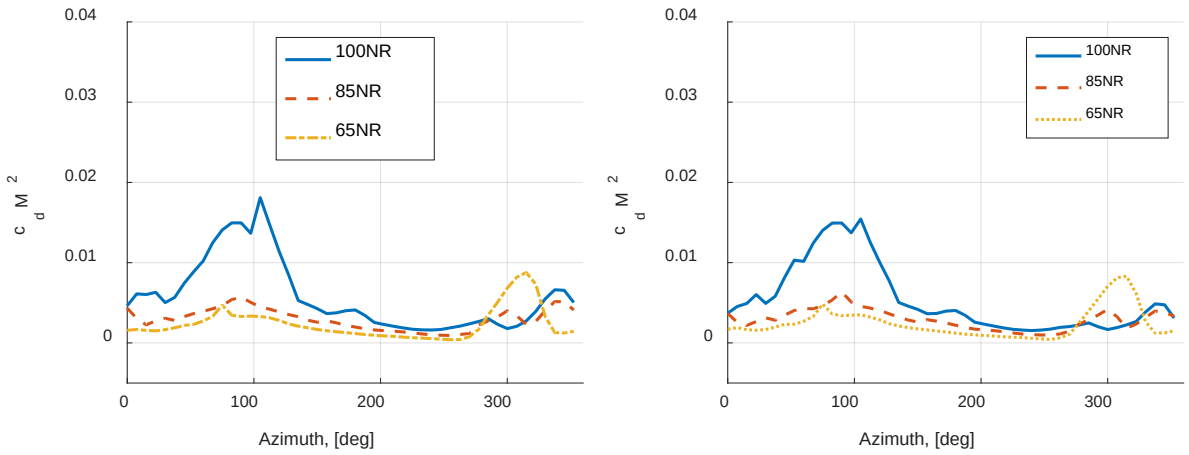

(a) Nominal ($\theta = 25°$), 89%R **(b) Winckler ($\theta = 25°$), 95%R**

Figure 25. Drag as a function of azimuth comparing the nominal coupled spar design to the Winckler layup (where $\theta = 25°$) for 100NR, 85NR, and 65NR

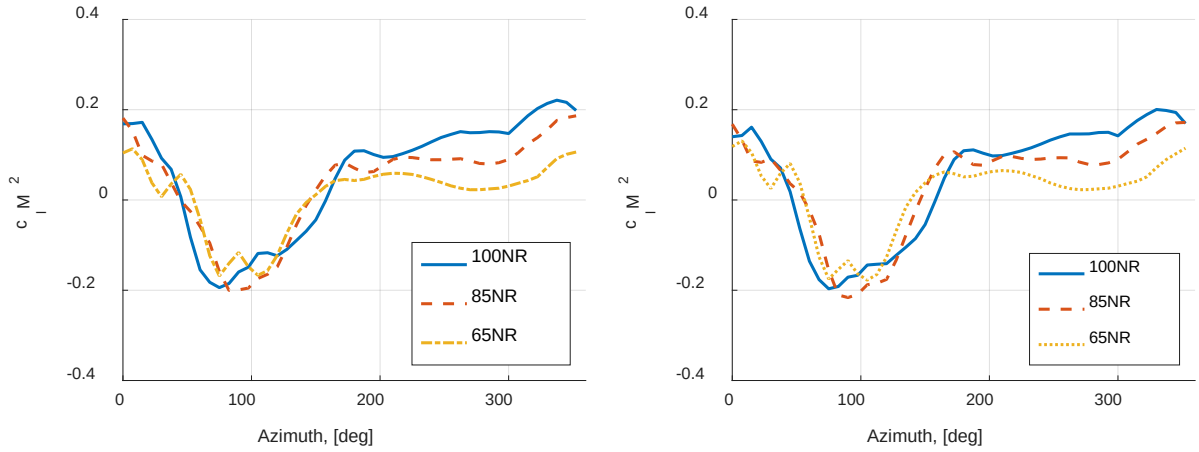

(a) Nominal ($\theta = 25°$), 89%R **(b) Winckler ($\theta = 25°$), 95%R**

Figure 26. Lift as a function of azimuth comparing the nominal coupled spar design to the Winckler layup (where $\theta = 25°$) for 100NR, 85NR, and 65NR

This gives confidence in the homogenization process. Additionally, the fiber strain is well within the allowables for IM7/8552. Figure 31 (b) shows the fiber strain at 25%R, along the advancing side of the rotor, and at a leading edge corner of the spar (reference Point B in Figure 29). At this area of high strain concentration it can be seen that the fiber direction strains still do not exceed the allowables.

The Winckler blade encounters higher strains at higher RPM as extension-torsion coupling is brought into play. As can be seen in Figure 28, there is greater overall axial strain towards the blade root compared to the uncoupled rotor, in Figure 27. In order to achieve the same twist as the uncoupled rotor at 100NR, the coupled rotor goes through a change of about 10° twist at the tip. As the rotor RPM is decreased, and the coupled blade begins to return to its cold shape (reduces the twist deformation), the large strains disappear, as shown in Figure 31.

CONCLUSIONS

A UH-60A-like metallic rotor spar was replaced with composite, IM7/8552 ply layups. Three extension-torsion coupled layups were analyzed, two of which were hygrothermally stable. The benefits of coupling were studied in detail, including the departure from the baseline titanium spar and the relative differences in the aerodynamics operating envelopes of all the blades. Strains were analyzed to determine whether they remained within the allowable limits for IM7/8552. Based on the current study, the following conclusions are drawn:

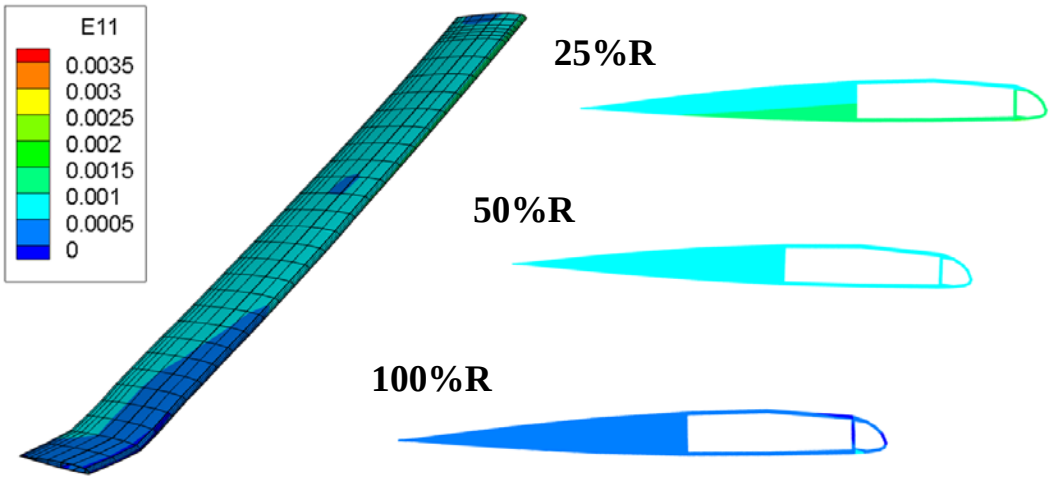

Figure 27. Axial strain in uncoupled rotor at 100NR, $\psi = 0°$ and cross sectional strain distribution at 1, 50, and 100%R

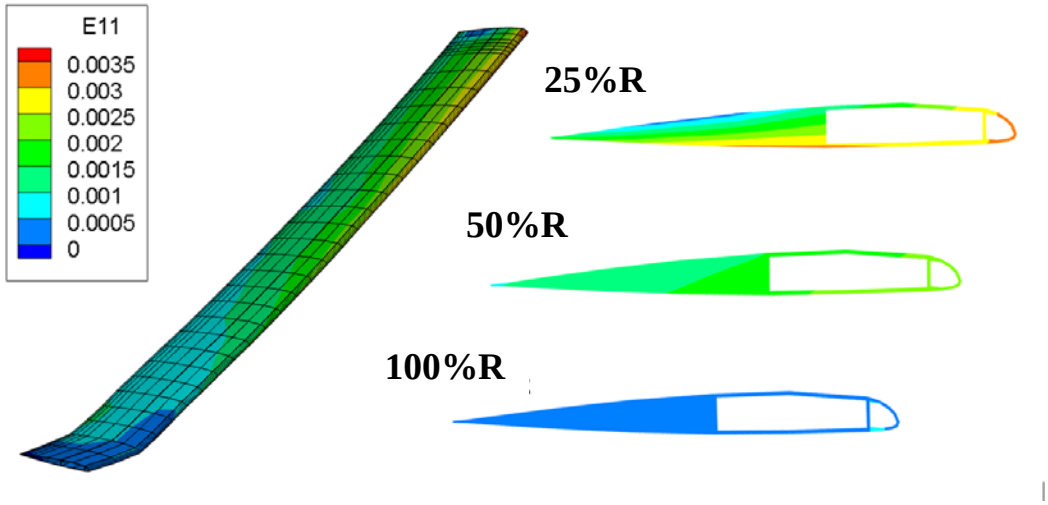

Figure 28. Axial strain in a Winckler coupled rotor at 100NR, $\psi = 0°$ and sectional strain distribution at 1, 50, and 100%R

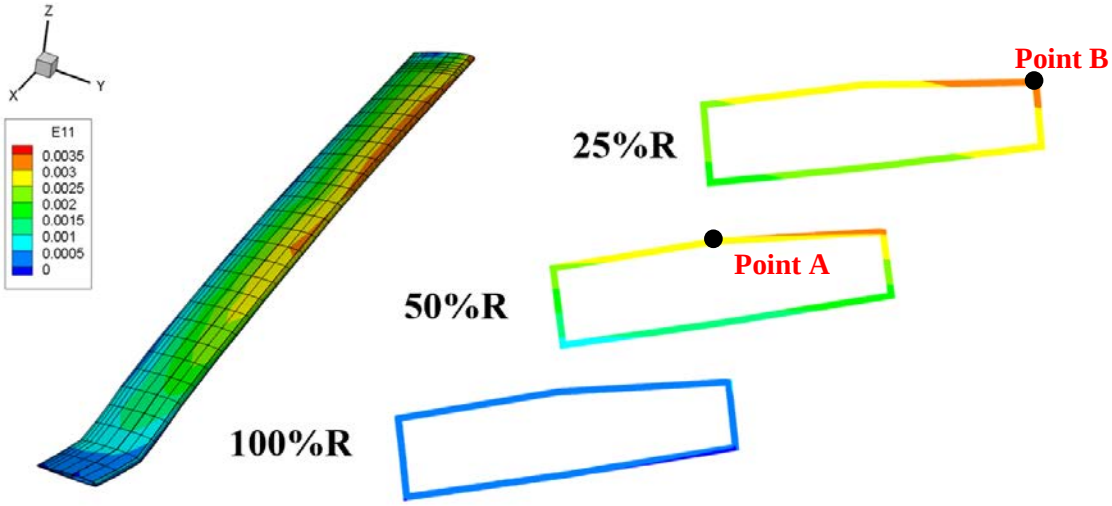

Figure 29. Axial strain in a Winckler coupled rotor at 100NR,$\psi = 97.5°$ where large axial strain in the spar is found

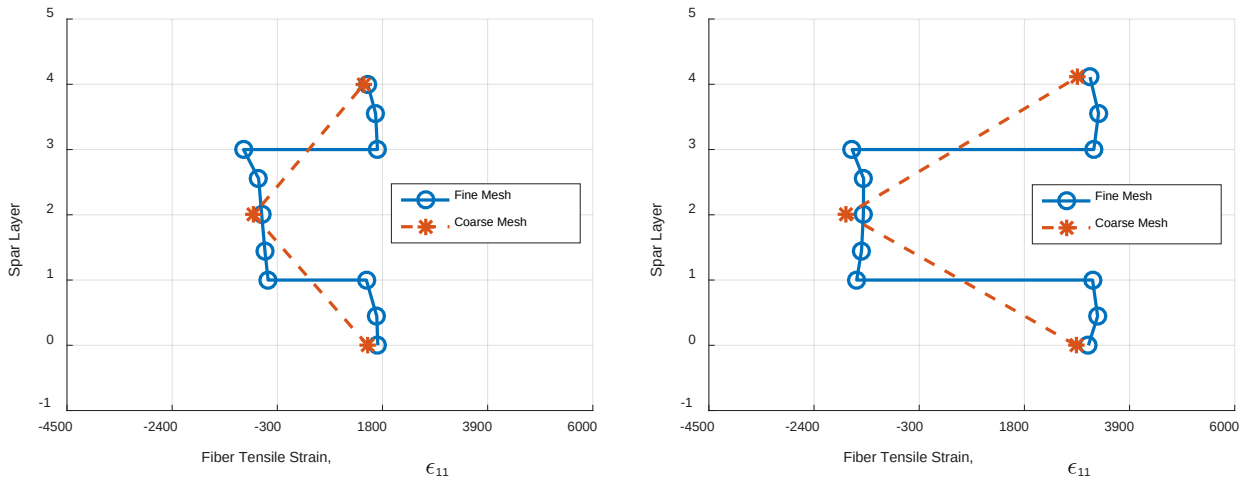

(a) Strain at at 50%R, Point A, and azimuth of $\psi = 0°$ (b) Strain at 25%R, Point B, and azimuth of $\psi = 97.5°$

Figure 30. Fiber tensile strain, ε_{11}, for ply resolved (fine mesh) and homogenized (coarse mesh) blades with a Winckler layup of $[25°/115°/115°/25°]$

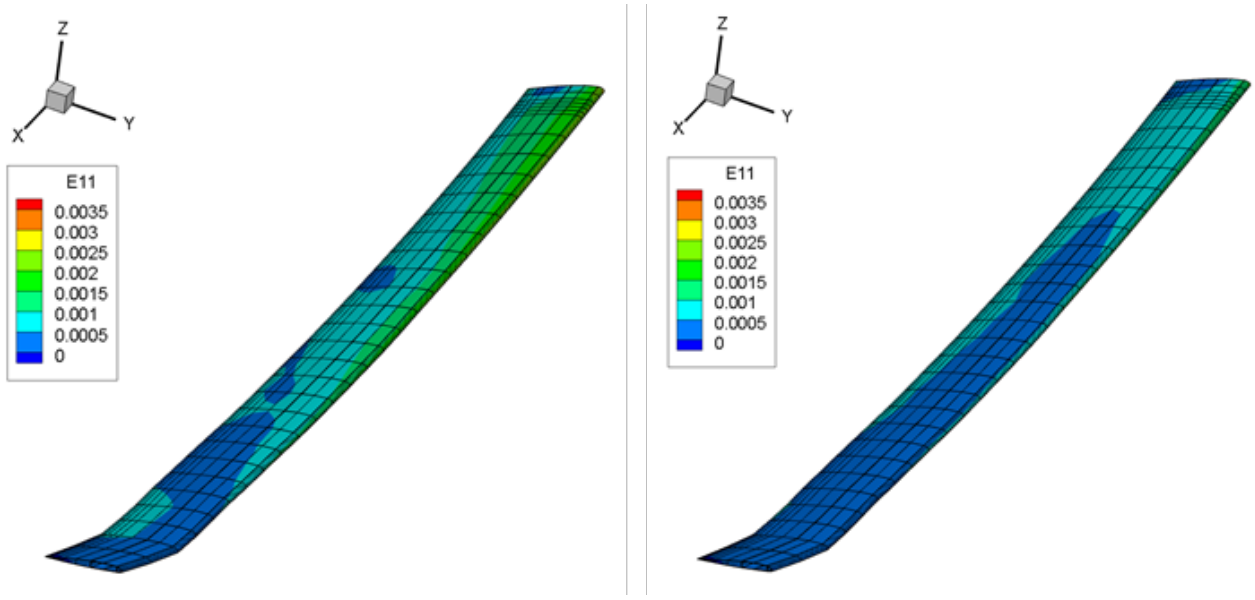

(a) 85NR **(b) 65NR**

Figure 31. Reduced axial strain for the Winckler rotor at 85NR and 65NR, at $\psi = 0°$

(i) It was determined that when the rotor is slowed to 85NR, the extension-torsion coupling from the nominal layup with $\theta = 45°$ provides enough twist differential from the 100NR case to provide an increase in rotor aerodynamic efficiency. As the uncoupled rotor does not untwist as the rotor slows it is well established that the twist plays a large role in this efficiency gain. It was also determined that the nominal composite coupling can only provide a performance boost for a certain range of operating RPMs and blade loading combinations.

(ii) It was shown that the use of hygrothermally stable extension-torsion coupled layups does not negatively impact rotor performance. At 85NR the Winckler layup performed equally as well as the nominal layup with an L/D_e of 8.14 at $C_T/\sigma \approx 0.1$, while the Haynes layup performed worse by a maximum L/D_e of 0.3 at $C_T/\sigma \approx 0.1$.

(iii) When the rotor RPM was reduced to 65NR, the Winckler rotor outperformed both the nominal and Haynes rotors by a maximum L/D_e of 0.3 and 0.5 respectively, at $C_T/\sigma \approx 0.09$.

(iv) The axial strain seen in the Winckler rotor falls within the allowable strain for IM7/8552 for RPMs up to 100NR. This strain was not found in the uncoupled rotor at 100NR (no change in twist) and was reduced as the rotor RPM slowed (less change in twist) so it is theorized that elastic twist and the extension needed to induce it play a key role in axial strain.

ACKNOWLEDGEMENTS

This work was performed at the University of Maryland Alfred Gessow Rotorcraft Center under Army Aeroflightdynamics Directorate funding through the Vertical Lift Research Center of Excellence (VLRCOE, grant number W911W61120012), with technical monitors Mahendra Bhagwat, Tom Maier, and Roger Strawn.

REFERENCES

[1] Ormiston, R. A., "Revitalizing Advanced Rotorcraft Research - and the Compound Helicopter," *Journal of the American Helicopter Society*, vol. 61, no. 1, pp. 1-23, January 2016.

[2] Johnson, W., Yamauchi, G. K. and Watts, M. E., "NASA Heavy Lift Rotorcraft Systems Investigation," NASA TP-2005-213467, Moffett Field, CA, December 1, 2005.

[3] Mahadev, S. and Dancila, D., "Extension-Twist-Coupled Star-Beam Composite Rotor Blade Tip Concept," in *in 18th International Conference on Composite Materials*, December 1, 2011.

[4] Datta, A. and Johnson, W., "Three-Dimensional Finite Element Formulation and Scalable Domain Decomposition for High Fidelity Rotor Dynamic Analysis," *Journal of the American Helicopter Society*, vol. 56, no. 2, pp. 1-14, 2011.

[5] Datta, A., "X3D - A 3-D Solid Finite Element Multibody Dynamic Analysis for Rotorcraft," in *Aeromechanics Specialists Conference*, San Francisco, CA, January 22, 2016.

[6] Datta, A. and Johnson, W., "Integrated Aeromechanics with Three-Dimensional Solid-Multibody Structures," in *70th Annual American Helicopter Society Forum Precedings*, Montreal, QC, May 20-22, 2014.

[7] Staruk, W., Weiner, E. and Chopra, I., "CAD-Based 3-D Structural Dynamic Modeling of the Tilt Rotor Aeroacoustic Model (TRAM) Proprotor," in *71st Annual Forum of the American Helicopter Society Precedings*, Virginia Beach, VA, May 5-7, 2015.

[8] Winckler, S., "Hygrothermally Curvature Stable Laminates with Tension-Torsion Coupling," *Journal of the American Helicopter Society*, vol. 30, no. 3, pp. 56-58, July 1985.

[9] Haynes, R. and Armanios, E., "Overview of Hygrothermally Stable Laminates with Improved Extension-Twist Coupling," in *17th International Conference on Composite Materials, ICCM-17*, Edinburgh, GBR, July 2009.

[10] Chou, P. C., Carleone, J. and Hsu, C. M., "Elastic Constants of Layered Media," *Journal of Composite Materials*, vol. 6, no. 1, pp. 80-93, 1972.

[11] Chandra, R., Stemple, A. D. and Chopra, I., "Thin-Walled Composite Beams Under Bending, Torsional, and Extensional Loads," *Journal of Aircraft*, vol. 27, no. 7, pp. 619-626, July 1990.

[12] Datta, A., Yeo, H. and Norman, T. R., "Experimental Investigation and Fundamental Understanding of a Slowed UH-60A Rotor at High Advance Ratios," *Journal of the American Helicopter Society*, vol. 58, no. 2, pp. 1-17, April 2013.

[13] Yeo, H., "Investigation of UH-60A Rotor Performance and Loads at High Advance Ratios," *Journal of Aircraft*, vol. 50, no. 2, pp. 576-589, March-April 2013.

[14] Potsdam, M., Yeo, H. and Ormiston, R., "Performance and Loads Predictions of a Slowed UH-60A Rotor at High Advance Ratios," in *39th European Rotorcraft Forum*, Moscow, Russia, Sept. 2013.

[15] Kosmatka, J. L. R., "Passive approach of controlling twist in composite tilt-rotor blades," in *SPIE Proceedings Vol. 2717*, May 1, 1996.

[16] Nixon, M. W., "Improvements to Tilt Rotor Performance Through Passive Blade Twist Control," NASA Technical Memorandum 100583, Hampton, VA, April 1988.

[17] Bagai, A., "Aerodynamic Design of the X2 TD Aircraft," in *American Helicopter Society 64th Annual Forum*, Montreal, Canada, April 29-May 1, 2008.

[18] Ozbay, S., Bauchau, O., Dancila, S. and Armanios, B., "Stability analysis of extension-twist coupled composite rotor blades," in *in 61st Annual Forum Proceedings - AHS Internationsl*, Grapevine, TX, June 1-3, 2005.

[19] Soykasap, O. and Hodges, D., "Performance Enhancement of a Composite Tilt-Rotor Using Aeroelastic Tailoring," *Journal of Aircraft*, vol. 37, no. 5, pp. 850-858, August 2000.

[20] Bauchau, O., Loewy, R. and Bryan, P., "An Approach to Ideal Twist Distribution in Tilt Rotor VSTOL Blade Designs," in *39th Annual Forum of the American Helicopter Society Precedings*, May 1983.